

Stability Analysis of a Virtual Synchronous Machine-based HVDC Link by Gear's Method

Jalal Khodaparast
Department of IEL
NTNU
Trondheim, Norway
jalal.khodaparast@ntnu.no

Olav Bjarte Fosso
Department of IEL
NTNU
Trondheim, Norway
olav.fosso@ntnu.no

Marta Molinas
Department of ITK
NTNU
Trondheim, Norway
marta.molinas@ntnu.no

Jon Are Suul
Department of ITK
NTNU and SINTEF
Trondheim, Norway
Jon.A.Suul@sintef.no

Abstract—Declining equivalent inertia caused by the massive integration of converter-based technologies can increase the risk of stability problems in the future power system. Control of HVDC systems as Virtual Synchronous Machines (VSMs) for providing emulated inertia is a promising countermeasure against this development. However, low inertia converter-dominated power systems are raising new challenges for stability analysis. Thus, new numerical techniques and tools are needed for efficient and accurate analysis of small- and large-signal stability issues in complex power systems with different kinds of generation units, converter systems and control loops that can experience potential interactions, internally or with the network. Gear's method with a variable time step, offers the possibility to obtain fast and flexible procedures for large-signal stability analysis. Additionally, it can make stability analysis efficient by combining the small-signal and large-signal analysis into the same process. This paper will show how the stability of a power system with a VSM-based HVDC link can be evaluated by the method and presents an approach for simultaneous small- and large-signal stability assessment.

Keywords—Gear's method, HVDC transmission, Large-signal stability, Small-signal stability, Virtual Synchronous Machines.

I. INTRODUCTION

Growing energy consumption and concerns about environmental issues are contributing to an intensive attention on renewable energy resources. In recent years, there is an ongoing growth in utilization of different renewable energy sources, and power electronics converters are usually applied to integrate them to the main power system. For the power electronics-fed renewable energy resources, converters decouple the electrical system from the mechanical system. This may decrease the total equivalent inertia of converter-dominated power systems [1].

Inertia is an inherent property of any system that resists changes in its speed or rotation. In classical power systems, the rotating generation units provide the inertia which prevent instantaneous changes in frequency. While synchronous condensers can be utilized to compensate for reduced system-level inertia due to reduced share of traditional synchronous generators (SGs), this is a costly solution for large power systems. However, converters for High Voltage Direct Current (HVDC) transmission can be controlled to emulate the inertial response of SGs [2]–[4]. If the converter control system includes a simulation of an SG swing equation, it is commonly

labelled as a Virtual Synchronous Machine (VSM) [5]. Such control methods can also provide damping for oscillations in the power system [4], [6]. Additionally, VSM-based control of converters is suitable in a smart grid context since it is not relying on synchronization to a stiff power system. However, small- and large-signal stability analysis of such systems need development of new numerical techniques and tools. While electrical power systems models are becoming more and more complex, simulation of the system becomes prone to numerical instability. Therefore, appropriate time steps should be carefully adopted [7]. Traditional methods for fixed time-step numerical integration requires the time step to be smaller than the smallest time constant in the dynamics of the power system. This requirement makes it difficult to address the stability issues of a complex large-scale power system. Variable time steps will enable a procedure of stability analysis by reducing the computation time. Gear's method implements an algorithm based on a predictor and corrector scheme which is a promising method to automatically adjust the step size of the numerical analysis [8]. Although variable-time-step methods are also available in MATLAB and EMT-like (ElectroMagnetic Transients) programs, they are limited by the fundamental frequency of the system, since all dynamic models are implemented in a stationary frame. However, Gear's method deals with a dynamic-algebraic system, which in addition to the combined EMT-like and phasor-based simulation, takes advantage of a dq-representation. Therefore, the way of implementing variable-time step simulation of hybrid dq and phasor models by the Gear's method has advantages compared to methods implemented in the stationary frame.

AC/DC power systems are typically complex systems that can be labeled as a stiff system in numerical analysis. Stiffness is an efficiency concept that shows there is a wide range of time constants in the system [9]. A stiff system needs a stiff solver where the numerical stability is ensured. The proposed method in this paper is a second-order predictor-corrector method and performs the integration efficiently by adapting the step size automatically [10]. Moreover, this method has the potential to perform the small- and large-signal analysis as a unified procedure. Additionally, it is a hybrid method that can deal with both phasor models and detailed (dynamic) models of the power system components. For a large-scale power

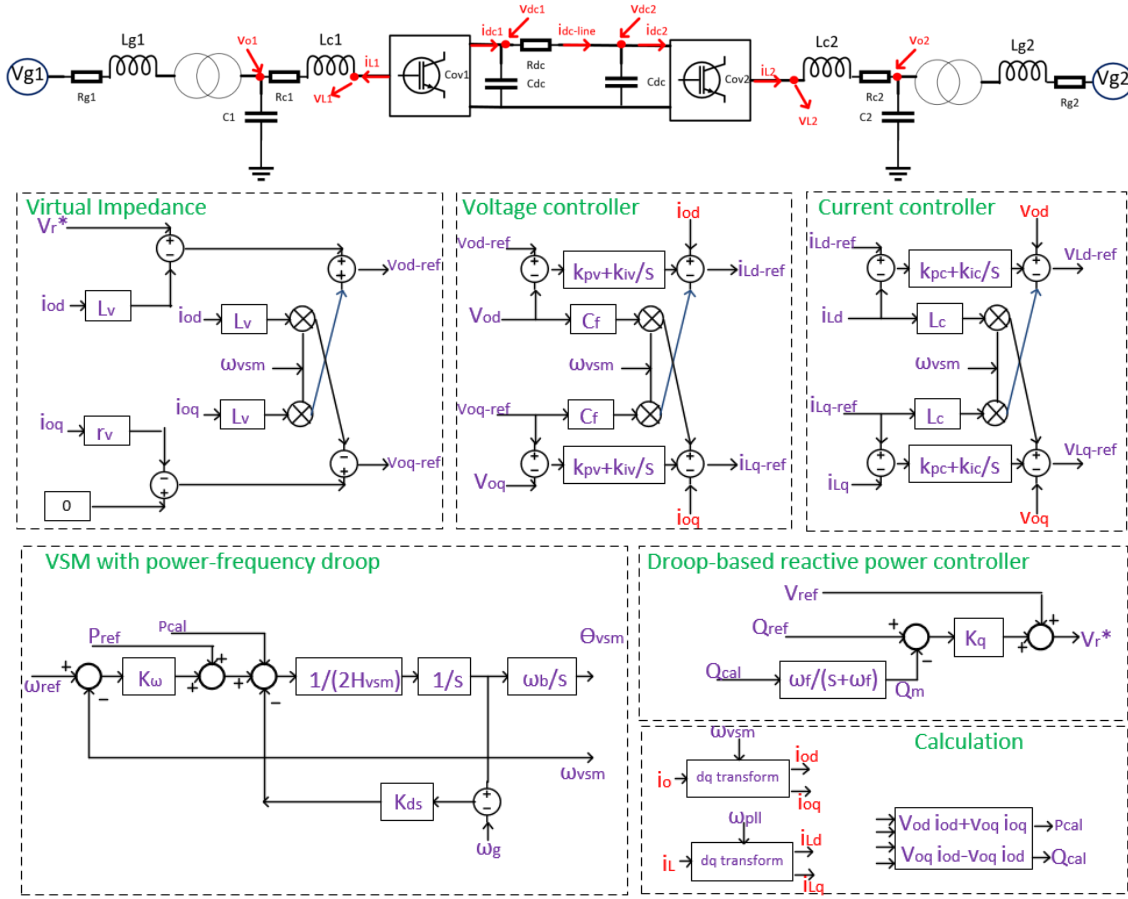


Fig. 1. Electrical and control parts of a VSM-based HVDC link

system with many elements, the hybrid capability improves the efficiency of the stability analysis [11], [12].

II. MODELS OF GENERATOR AND VSM-CONTROLLED HVDC

In this paper, generators and VSM-controlled HVDC converters are modeled dynamically. The system equations are used by the Gear's method to evaluate dynamic performance of the system subjected to non-severe and severe disturbances. A brief description of the dynamic models (generator and VSM-controlled HVDC link) is represented in this section.

A. Generator model

In classical model of a generator, it is represented by a voltage source (constant-amplitude and time-varying-angle) behind a transient reactance (x'_d). The generator is then represented by the swing equation as

$$\begin{aligned} \frac{d}{dt} \Delta\omega_r &= \frac{0.5}{H_{int}} (P_m - P_e - K_D \Delta\omega_r) \\ \frac{d}{dt} \delta &= \omega_0 \Delta\omega_r \end{aligned} \quad (1)$$

where ω_r is rotor's angular frequency, H_{int} is inertia constant, P_m and P_e are mechanical and electrical powers, δ is load angle, ω_0 is nominal angular frequency.

B. Model of VSM-controlled HVDC link

The VSM-controlled HVDC link consists of electrical (AC and DC) and control parts, of which the dynamic models are presented here. The HVDC converter terminals are represented by a traditional Voltage Source Converter (VSC) modeled by equations as:

$$\begin{aligned} \frac{d}{dt} i_{Ld} &= \frac{\omega_g \omega_b}{L_c} v_{Ld} - \frac{\omega_g \omega_b}{L_c} v_{od} - \frac{\omega_g \omega_b R_c}{L_c} i_{Ld} + \omega_g \omega_b i_{Lq} \\ \frac{d}{dt} i_{Lq} &= \frac{\omega_g \omega_b}{L_c} v_{Lq} - \frac{\omega_g \omega_b}{L_c} v_{oq} - \frac{\omega_g \omega_b R_c}{L_c} i_{Lq} - \omega_g \omega_b i_{Ld} \\ \frac{d}{dt} v_{dc} &= \omega_g \omega_b C_{dc} (\pm i_{dc} \mp i_{dc-line}) \end{aligned} \quad (2)$$

Parameters and variables presented in (2) are represented in per-unit quantities, and are identified in Fig.1, where parameters and variables of the rectifier-side are labeled by '1' while the inverter-side variables are labeled by '2'. However, in (2), the rectifier- and inverter-side equations are defined by \pm and \mp , respectively. The grid and base angular frequencies are denoted as ω_g and ω_b . In addition to the electrical part, control part of VSM-controlled HVDC link should be modeled dynamically. The applied VSM-based control strategy includes cascaded current and voltage controllers as shown in Fig.1

[13]. The equations defining the current controller are:

$$\begin{aligned} v_{Ld-ref} &= k_{pc}(i_{Ld-ref} - i_{Ld}) + k_{ic}\gamma_{id} + v_{od} - \omega_{vsm}L_c i_{Lq} \\ v_{Lq-ref} &= k_{pc}(i_{Lq-ref} - i_{Lq}) + k_{ic}\gamma_{iq} + v_{oq} + \omega_{vsm}L_c i_{Ld} \\ \frac{d}{dt}\gamma_{id} &= i_{Ld-ref} - i_{Ld} \\ \frac{d}{dt}\gamma_{iq} &= i_{Lq-ref} - i_{Lq} \end{aligned} \quad (3)$$

where γ_{id} and γ_{iq} represent the integrator states of the PI-controllers. Parameters and variables presented in (3) are shown in Fig.1. The voltage controller is modelled as:

$$\begin{aligned} i_{Ld-ref} &= k_{pv}(v_{od-ref} - v_{od}) + k_{iv}\gamma_{vd} + i_{od} - \omega_{vsm}C_f v_{Lq} \\ i_{Lq-ref} &= k_{pv}(v_{oq-ref} - v_{oq}) + k_{iv}\gamma_{vq} + i_{oq} + \omega_{vsm}C_f v_{Ld} \\ \frac{d}{dt}\gamma_{vd} &= v_{Ld-ref} - v_{Ld} \\ \frac{d}{dt}\gamma_{vq} &= v_{Lq-ref} - v_{Lq} \end{aligned} \quad (4)$$

where γ_{vd} and γ_{vq} represent the integrator states. Parameters and variables presented in (4) are shown in Fig.1. The reactive power control and the virtual impedance presented in Fig.1 are modeled as:

$$\begin{aligned} \frac{d}{dt}q_m &= -\omega_f q_m + \omega_f Q_{cal} \\ Q_{cal} &= v_{oq}i_{od} - v_{od}i_{oq} \\ V_r^* &= v_{ref} - K_q(Q_{ref} - Q_{cal}) \\ v_{od-ref} &= V_r^* - r_v i_{od} + \omega_{vsm}l_v i_{oq} \\ v_{oq-ref} &= 0 - r_v i_{oq} - \omega_{vsm}l_v i_{od} \end{aligned} \quad (5)$$

Contrary to the conventional control of VSC- HVDC systems, where a Phase Locked Loop (PLL) is used to specify the angle reference for the converter, control based on VSM creates the reference angle based on simulating the dynamic model of synchronous machine (similar to equation presented in (1)) for the converter. The dynamic equations of the rectifier converter for the VSM-based control are:

$$\begin{aligned} \frac{d}{dt}\Delta\omega_{vsm1} &= \frac{0.5}{H_{vsm}} \times \\ & (P_{ref} - P_{cal} - K_{ds}\Delta\omega_{vsm1} + K_w(\omega_{ref1} - \omega_{vsm1})) \\ \frac{d}{dt}\delta\theta_{vsm1} &= \omega_b \Delta\omega_{vsm1} \\ P_{cal} &= v_{od}i_{od} + v_{oq}i_{oq} \end{aligned} \quad (6)$$

where the parameters are shown in Fig.1 and $K_{ds}\Delta\omega_{vsm1}$ represents the damping. On the other hand, the inverter of the VSM-based HVDC link is modeled as [4]:

$$\begin{aligned} \frac{d}{dt}\Delta\omega_{vsm2} &= \frac{0.5}{H_{vsm}} \times \\ & (v_{dc-ref} - v_{dc} - K_{ds}\Delta\omega_{vsm2} + K_w(\omega_{ref2} - \omega_{vsm2})) \\ \frac{d}{dt}\delta\theta_{vsm2} &= \omega_b \Delta\omega_{vsm2} \end{aligned} \quad (7)$$

Therefore, generator and VSM-based HVDC link are modeled by the equation presented in section II (A,B).

C. Integration of VSM-based HVDC link to a power system

The current injection method is used in this paper to integrate the dynamic model of the VSM-based HVDC link to the power system [14], [15]. According to the injected current method, the injected currents (I_g for generator buses and I_x for non-generator buses) and voltages of buses (V_g for generator buses and V_x for non-generator buses) are related as:

$$\begin{pmatrix} I_g \\ I_x \end{pmatrix} = \begin{pmatrix} Y_K & Y_L \\ Y_L^T & Y_M \end{pmatrix} \begin{pmatrix} V_g \\ V_x \end{pmatrix} \quad (8)$$

Since the interactions of the VSM-based HVDC link with the whole system is investigated in this paper, the I_x is a nonzero vector (it is zero in a classical power system without HVDC), and two nonzero arrays ($io1$ and $io2$) are formed in the vector. These are injected currents by the VSM-based HVDC link at two points of common couplings (PCCs). Therefore, with the VSM-controlled HVDC link connecting Bus k (conv1) and Bus j (conv2), the bus voltages and generator currents are calculated as:

$$\begin{aligned} \begin{pmatrix} ioD \\ ioQ \end{pmatrix} &= \begin{pmatrix} \cos(\delta\theta_{pll}) & -\sin(\delta\theta_{pll}) \\ \sin(\delta\theta_{pll}) & \cos(\delta\theta_{pll}) \end{pmatrix} \begin{pmatrix} iod \\ iod \end{pmatrix} \\ I_x &= [0, 0, \dots, io1, io2, 0, \dots, 0] \\ V_x &= Y_M^{-1}(I_x - Y_L^T V_g) \\ V_{Bus-k} &= V_x(k), \quad V_{Bus-j} = V_x(j) \\ I_g &= Y_K V_g + Y_L V_x \end{aligned} \quad (9)$$

III. GEAR'S METHOD

The equations presented in the previous section model the whole system as an Differential-Algebraic Equation (DAE) system. The Gear's method as a numerical integration method is applied to the DAE system to approximate the excursion of state variables during severe and non-severe disturbances. The method is a second-order numerical integration method that operates on prediction and correction stages. It adjusts the integration step size based on the instantaneous stiffness of the equations to fulfill the desired accuracy. It uses second-order Taylor expansion to predict the variables in the prediction stage and uses a Newton-Raphson method to correct the predictions in the correction stage [8], [10]. A general nonlinear DAE system has the form as

$$\begin{aligned} y' &= f(y, x, t) \\ 0 &= g(y, x, t) \end{aligned} \quad (10)$$

where y and f are differential variable and function, x and g are algebraic variable and function and t is time. In the prediction stage of the method, the next step solution y_{n+1} and its first and second derivatives are predicted by the Taylor expansion as [16]

$$\begin{aligned} y_{n+1}^P &= y_n + H_{n+1} y_n' + H_{n+1}^2 y_n''/2 \\ y_{n+1}^{P'} &= y_n' + H_{n+1} y_n'' \\ y_{n+1}^{P''} &= y_n'' \end{aligned} \quad (11)$$

where H is the integral step size, y' and y'' are first and second derivatives. In the correction stage of the method, the predicted values are corrected as

$$\begin{aligned} y_{n+1} &= y_{n+1}^P + \Delta y \\ y'_{n+1} &= y'_{n+1}^P + \Delta y I_1/H_{n+1} \\ y''_{n+1} &= y''_{n+1}^P + 2\Delta y I_2/H_{n+1}^2 \end{aligned} \quad (12)$$

where $I_1 = (2H_{n+1} + H_n)/(H_{n+1} + H_n)$ and $I_2 = (H_{n+1})/(H_{n+1} + H_n)$ are constant values, which depend on the integral step size. Δy is the difference between the predicted and the corrected values. To solve the differential equation presented in (10), the method defines a new function U based on (10) and (12). U_{n+1} is extracted from the main nonlinear differential equation presented in (10) and the corrected value of first derivative (y'_{n+1}) presented in (12) as

$$U_{n+1} = y'_{n+1} - f(y_{n+1}, x_{n+1}, t_{n+1}) = 0 \quad (13)$$

$$U_{n+1} = H_{n+1} y'_{n+1}^P + I_1 \Delta y + \dots$$

$$\dots - H_{n+1} f(y_{n+1}^P + \Delta y, x_{n+1}^P + \Delta x, t + H_{n+1}) = 0$$

A system of DAEs (where U is a new defined differential equation presented in (13) and g is the algebraic equation presented in (10)) can be converted to a system of Ordinary Differential Equation (ODE) by differentiating it with respect to the variables as

$$\begin{pmatrix} U_{n+1} \\ g_{n+1} \end{pmatrix} = \begin{pmatrix} I_1 - H \frac{\partial f}{\partial y} & -H \frac{\partial f}{\partial x} \\ \frac{\partial g}{\partial y} & \frac{\partial g}{\partial x} \end{pmatrix} \begin{pmatrix} \Delta y \\ \Delta x \end{pmatrix} \quad (14)$$

where Δx is the difference of predicted and corrected values of the algebraic variable. The only unknown variables in (14) are Δy and Δx , which are computed by finding the roots of the system ($U_{n+1} = 0$, $g_{n+1} = 0$). Newton-Raphson is a well-known method for finding the roots of coupled nonlinear equations. Thus, changes of variables (Δx and Δy) to approximate the next step solution are calculated by solving (14). The partial derivatives of the differential and algebraic functions with respect to the variables ($\frac{\partial f}{\partial x}$, $\frac{\partial g}{\partial x}$, $\frac{\partial g}{\partial y}$) presented in (14) can form the time-varying state matrix (A-matrix) of nonlinear system as:

$$A = \frac{\partial f}{\partial y} - \left(\frac{\partial f}{\partial x} \left(\frac{\partial g}{\partial x} \right)^{-1} \frac{\partial g}{\partial y} \right) \quad (15)$$

This characteristic of the proposed method makes it a more powerful solver capable of providing small-signal stability analysis as an additional function during numerical integration for large-signal stability analysis.

In the updating stage of the method, the integral step size is adjusted by an internal loop based on the approximation error. According to the adaptive step size strategy, accuracy

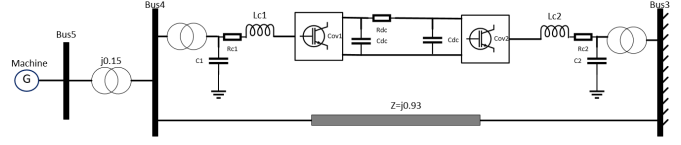


Fig. 2. Single Machine to Infinite Bus (SMIB) with VSM-based HVDC link

of the approximation is checked by the Truncation Error (TE) defined by (16).

$$TE = |z(t_{n+1}) - z_{n+1}| = 2K_2 I_2 \|\Delta z\| \quad (16)$$

where $z = [y, x]$ is a global variable including both differential and algebraic variables and $K_2 = (1/6)(H_{n+1} + H_n)^2/(H_{n+1}(2H_{n+1} + H_n))$. Based on the calculated TE, the integral step size of the algorithm is adapted as [16]

$$H_{new} = K_{sc} \sqrt{\frac{TE_{ds}}{2K_2 I_2 \|\Delta z\|}} H_{old} \quad (17)$$

where TE_{ds} is the desired accuracy. K_{sc} is a scaling that is set to lower than one when decreasing the step size and is bigger than one when increasing the step size. According to the internal procedure of the method, it introduces a new approach to detect large-signal instability in the numerical simulation of a power system. TE of a stable system is always lower than TE_{max} , but it exceeds this limit during unstable conditions due to the divergence of the numerical solutions. Therefore, monitoring the truncation error is utilized in this paper to discriminate the stable from the unstable conditions.

IV. SIMULATION RESULTS

A Single Machine to Infinite Bus (SMIB) with VSM-controlled HVDC link is used in this section to evaluate the performance of the proposed method in a converter-based power system. The power system without the HVDC link is presented in [9]. The generator (G1) shown in Fig.2 produces an apparent power $S_{Bus1} = 0.9 + j0.436$ (in per-unit) at Bus1 with voltage $V_{Bus1} = 1.0 \angle 28.34^\circ$ during steady state. The generator is presented by a second-order model with an internal voltage ($E' \angle \delta$) behind a transient reactance $X'_d = 0.3 p.u.$, inertia constant $H_{int} = 3.5s$ and damping factor $K_D = 2$. It is connected to an infinite bus ($V_{Bus3} = 0.90081 \angle 0$) through the network, which is shown in Fig.2.

One of two transmission lines in the network is the VSM-controlled HVDC link from section II.B. Reference values of the Rectifier-side (Conv1, Bus2) of the HVDC link are: $P_{ref1} = -0.5853$, $Q_{ref1} = -0.1860$, $V_{ref1} = 1$ and $\omega_{ref1} = 1$ and the reference values of the Inverter-side (Conv2, Bus3) of the HVDC link are: $v_{dc-ref2} = 1$, $Q_{ref2} = -0.0255$, $V_{ref2} = 0.90081$ and $\omega_{ref2} = 1$ (all in per-unit). The operating point is selected based on the steady-state condition of the SMIB system in [9] without the HVDC link. The parameters of the VSM-controlled terminals are: $k_{pv} = 5.9$, $k_{iv} = 70.36$, $k_{pc} = 2.54$, $k_{ic} = 28.6$, $H_{vsm} = 0.01$, $k_{ds} = 25$, $k_{\omega} = 0.2$, $k_q = 0.4$, $\omega_f = 1000$, $r_v = 0.1$, $l_v = 0.1$.

TABLE I
SMALL SIGNAL ANALYSIS OF HVDC LINK WITH CONVENTIONAL AND
VSM-BASED CONTROL

Number	Eigenvalue (conv. control)	Eigenvalue (VSM-controlled)
1	$10^3 \times (-0.0190 + 1.2155i)$	$10^3 \times (-0.4862 + 7.0959i)$
2	$10^3 \times (-0.0190 - 1.2155i)$	$10^3 \times (-0.4862 - 7.0959i)$
3	$10^3 \times (-0.0003 + 0.5713i)$	$10^3 \times (-0.6298 + 2.5037i)$
4	$10^3 \times (-0.0003 - 0.5713i)$	$10^3 \times (-0.6298 - 2.5037i)$
5	$10^3 \times (-0.0125 + 0.8826i)$	$10^3 \times (-0.8230 + 1.9710i)$
6	$10^3 \times (-0.0125 - 0.8826i)$	$10^3 \times (-0.8230 - 1.9710i)$
7	$10^3 \times (-0.0117 + 0.8081i)$	$10^3 \times (-0.6308 + 3.4783i)$
8	$10^3 \times (-0.0117 - 0.8081i)$	$10^3 \times (-0.6308 - 3.4783i)$
9	$10^3 \times (-0.0425 + 0.0000i)$	$10^3 \times (-1.0176 + 3.2144i)$
10	$10^3 \times (-0.0299 + 0.0000i)$	$10^3 \times (-1.0176 - 3.2144i)$
11	$10^3 \times (-0.0295 + 0.0000i)$	$10^3 \times (-1.8620 + 0.0000i)$
12	$10^3 \times (-0.0243 + 0.0000i)$	$10^3 \times (-2.1337 + 0.0000i)$
13	$10^3 \times (-0.0211 + 0.0000i)$	$10^3 \times (-0.1541 + 1.3482i)$
14	$10^3 \times (-0.0217 + 0.0000i)$	$10^3 \times (-0.1541 - 1.3482i)$
15	$10^3 \times (-0.0202 + 0.0000i)$	$10^3 \times (-1.2163 + 0.0000i)$
16	$10^3 \times (-0.0029 + 0.0001i)$	$10^3 \times (-1.2501 + 0.0000i)$
17	$10^3 \times (-0.0029 - 0.0001i)$	$10^3 \times (-0.4253 + 0.0000i)$
18	$10^3 \times (-0.0004 + 0.0021i)$	$10^3 \times (-0.0302 + 0.0000i)$
19	$10^3 \times (-0.0004 - 0.0021i)$	$10^0 \times (-1.0630 + 5.8054i)$
20	$10^3 \times (-0.0022 + 0.0000i)$	$10^0 \times (-1.0630 + 5.8054i)$
21	$10^3 \times (-0.0017 + 0.0000i)$	$10^2 \times (-0.00025 + 0.0619i)$
22	$10^3 \times (-0.0017 - 0.0000i)$	$10^2 \times (-0.00025 - 0.0619i)$
23	$10^0 \times (-0.0766 + 5.3803i)$	$10^3 \times (-0.0127 + 0.0000i)$
24	$10^0 \times (-0.0766 - 5.3803i)$	$10^3 \times (-0.0127 + 0.0003i)$
25	$10^3 \times (-0.0000 + 0.0001i)$	$10^3 \times (-0.0127 - 0.0003i)$
26	$10^3 \times (-0.0000 - 0.0001i)$	$10^3 \times (-0.0122 + 0.0000i)$
27	$10^3 \times (-0.0002 + 0.0000i)$	$10^3 \times (-0.0115 + 0.0000i)$
28	$10^3 \times (-0.0002 + 0.0000i)$	$10^3 \times (-0.0112 + 0.0000i)$
29	-	$10^3 \times (-0.0111 + 0.0002i)$
30	-	$10^3 \times (-0.0111 - 0.0002i)$

Gear's method is applied to the power system and the A-matrix of the system is extracted in every step time by the proposed method. The eigenvalues of the A-matrix in steady state condition are calculated and tabulated in Table I (Eigenvalue (VSM-controlled)). Since there are 30 differential equations in the whole model of the VSM-based HVDC link, 30 eigenvalues are calculated.

To compare the operation of the studied system with a VSM-based and a conventional control strategy for the VSC HVDC link, the eigenvalues for both cases are shown in Table I. The 28 eigenvalues are obtained from the dynamic model of the system with conventional control since the system is modeled with 28 differential equations. The dynamic model of the conventional control is presented in [17]. The rectifier-side (Conv1) of HVDC controls the active (P_1) and the reactive power (Q_1), while the inverter-side (Conv2) controls the DC voltage (v_{dc2}) and reactive power (Q_2). In steady-state conditions, reference values of the HVDC are: $P_{ref1} = -0.5853$, $Q_{ref1} = -0.1860$, $v_{dc2} = 1$ and $Q_{ref2} = -0.0255$ (all are in per unit). According to the Table I, the eigenvalue 19 and 20 in VSM-controlled HVDC, which is associated to the electro-mechanical oscillation has a bigger negative real value compared to the eigenvalue 23 and 24 in conventional PLL-based HVDC (also associated to the electro-mechanical oscillation of the power system).

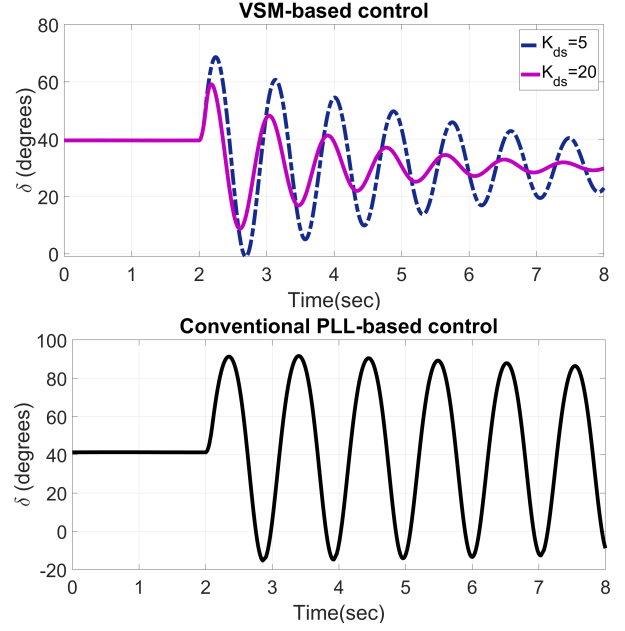


Fig. 3. VSC-HVDC with VSM-based and conventional control

To clarify the appropriate performance of the VSM-controlled HVDC in SMIB, the system is simulated for different values of K_{ds} ($K_{ds} = 5s$ and $20s$) and the results are shown in Fig.3. A three-phase fault occurred at Bus 2 at $t = 2s$ and is cleared by removing the transmission line with impedance $j0.93$. Additionally, the same disturbance is also applied to the power system with conventional HVDC control and the result are shown in the same figure. The simulation results show that the VSM-controlled HVDC link provides more damping for the oscillations compared to the conventional HVDC control.

The proposed method in this paper detects the instability by the TE and by this evaluates the large signal stability of the power system. According to the proposed technique, the transient performance of the power system subjected to a severe disturbance is evaluated numerically. The power system is simulated for three different fault duration ($T_{FC} = 0.1, 0.16, 0.17s$), and the results are shown in Fig.4. A three-phase fault occurred at Bus 2 at $t = 2s$ and is cleared after the fault duration.

The results presented in Fig.4 show that the system is stable with $T_{FC} = 0.10s$ and $T_{FC} = 0.16s$, but is unstable with $T_{FC} = 0.17s$. Therefore, the critical clearing time (CCT) is $0.16s$ for this disturbance. The TE for different conditions are also shown in Fig.4. The detection of the unstable conditions is based on the TE by monitoring the accuracy of numerical integration. Indeed, TE is always smaller than TE_{max} (except in the instant of fault occurrence and the disconnection) when the system is stable, but it will be bigger when the system is unstable. Finally, the critical clearing time for the conventional HVDC control is also evaluated and presented in Table II. According to the Table II, VSM-based HVDC control

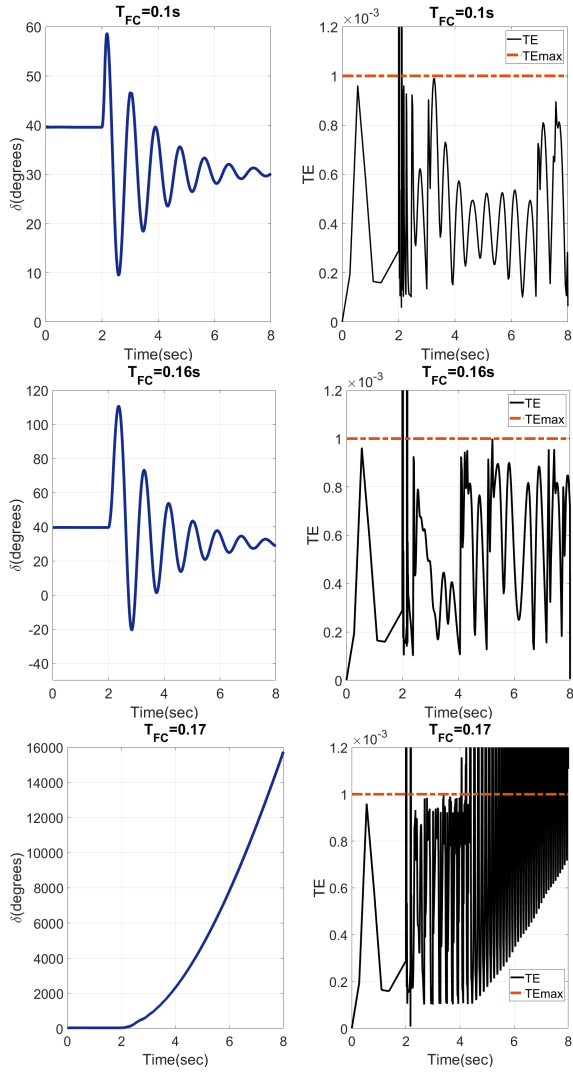


Fig. 4. Performance of VSM-based HVDC under severe disturbances

TABLE II
CRITICAL CLEARANCE TIME

system	T_{FC}
HVDC with conventional PLL-based control	0.1s
HVDC with VSM-based control	0.16 s

increases the critical clearing time and thereby improves the large-signal stability of the system. The presented results show that the proposed method can unify the small-signal and large-signal stability analysis of a power system into the same process and therefore increase the efficiency of the analysis.

V. CONCLUSION

A power systems with HVDC interconnections is a stiff system with a wide range of time constants, which needs a stiff solver for simulation-based large-signal stability analysis. Gear's method is proposed in this paper to analyze the stability efficiently by using a self-adaptive step size strategy. Analysis based on the self-adaptive time step is a promising concept that

can be used to reduce computation time. With time-varying time step, dynamics with significantly different time constants can be evaluated, and the speed of the calculations can be increased while the accuracy is preserved. Unified stability analysis (simultaneous small- and large-signal stability) of the system is achieved by the method in this paper. The small-signal analysis is performed during numerical integration by extracting the A-matrix of a power system and calculating the eigenvalues in the steady state conditions. Additionally, a new method for detecting unstable conditions is proposed by shedding light on the internal procedure of a numerical integration solver. Two cases of HVDC links with VSM-controlled and conventional PLL-controlled are simulated by the method, and the results show the appropriate performance of the proposed method in the stability analysis of a complex power system.

REFERENCES

- [1] M. CABIATI, "Synthetic inertia in wind power systems with dfigs and hvdc connections. analysis and simulations of some control systems," 2015.
- [2] J. Zhu, C. D. Booth, G. P. Adam, and A. J. Roscoe, "Inertia emulation control of vsc-hvdc transmission system," in *2011 International Conference on Advanced Power System Automation and Protection*, vol. 1. IEEE, 2011, pp. 1–6.
- [3] J. Huang and R. Preece, "Hvdc-based fast frequency support for low inertia power systems," 2017.
- [4] R. Aouini, B. Marinescu, K. B. Kilani, and M. Elleuch, "Synchronverter-based emulation and control of hvdc transmission," *IEEE Transactions on Power Systems*, vol. 31, no. 1, pp. 278–286, 2015.
- [5] S. D'Arco and J. A. Suul, "Virtual synchronous machines—classification of implementations and analysis of equivalence to droop controllers for microgrids," in *2013 IEEE Grenoble Conference*. IEEE, 2013, pp. 1–7.
- [6] L. A. Lopes *et al.*, "Self-tuning virtual synchronous machine: A control strategy for energy storage systems to support dynamic frequency control," *IEEE Transactions on Energy Conversion*, vol. 29, no. 4, pp. 833–840, 2014.
- [7] S. Kim and T. J. Overbye, "Optimal subinterval selection approach for power system transient stability simulation," *Energies*, vol. 8, no. 10, pp. 11 871–11 882, 2015.
- [8] O. B. Fosso, "Implementation of an implicit method for numerical integration of differential equations with self adaptive time step (gear's method)," DOI: 10.13140/RG.2.2.33826.43205.
- [9] P. Kundur, N. J. Balu, and M. G. Lauby, *Power system stability and control*. McGraw-hill New York, 1994, vol. 7.
- [10] A. H. G.D. Byrne, "A polyalgorithm for the numerical solution of ordinary differential equations," *ACM Transactions on Mathematical Software*, vol. 1, no. 1, pp. 71–96, 1975.
- [11] C. Karawita and U. Annakkage, "A hybrid network model for small signal stability analysis of power systems," *IEEE Transactions on power systems*, vol. 25, no. 1, pp. 443–451, 2009.
- [12] C. Karawita and U. D. Annakkage, "Multi-infeed hvdc interaction studies using small-signal stability assessment," *IEEE Transactions on Power Delivery*, vol. 24, no. 2, pp. 910–918, 2009.
- [13] S. D'Arco, J. A. Suul, and O. B. Fosso, "A virtual synchronous machine implementation for distributed control of power converters in smartgrids," *Electric Power Systems Research*, vol. 122, pp. 180–197, 2015.
- [14] H. Saadat *et al.*, *Power system analysis*, 1999.
- [15] L. Shen, "Model integration and control interaction analysis of ac/vsc hvdc system," Ph.D. dissertation, The University of Manchester (United Kingdom), 2015.
- [16] M. Stubbe, A. Bihain, J. Deuse, and J. Baader, "Stag-a new unified software program for the study of the dynamic behaviour of electrical power systems," *IEEE Transactions on Power Systems*, vol. 4, no. 1, pp. 129–138, 1989.
- [17] M. Amin, J. Suul, S. D'Arco, E. Tedeschi, and M. Molinas, "Impact of state-space modelling fidelity on the small-signal dynamics of vsc-hvdc systems," IET, 2015.